Effect of twin grain boundary on material thermal expansion

Yilin Zhang,[1] Huimin Mu,[1] Bangyu Xing,[1] Hongshuai Zou,[1] Yuhao Fu,[2,3,*] and Lijun Zhang[1,3,†]
[1]State Key Laboratory of Superhard Materials, Key Laboratory of Automobile Materials of MOE, College of Materials Science and Engineering, Jilin University, Changchun 130012, China
[2]State Key Laboratory of Superhard Materials, College of Physics, Jilin University, Changchun 130012, China
[3]International Center of Computational Method and Software, Jilin University, Changchun 130012, China

(Received 1 November 2021; accepted 20 July 2022; published 16 August 2022)

Based on first-principles phonon calculations within the framework of quasiharmonic approximation, we study the effect of twin grain boundary (TGB) on the thermal expansion of insulating materials. We select diamond-structure solids (C, Si, and Ge) and rutile (SnO_2) as representatives of the covalent and ionic bonding materials that are important systems commonly accompanied with TGB. We found distinct effects of TGB on thermal expansion in two types of materials. For diamond-structure solids, the thermal expansion of (111)-oriented twinning structure varies subtly from that of pristine material within the temperature range studied, which is primarily induced by the modification of vibrational phonon mode by the TGB effect. Distinctly, the thermal expansion of SnO_2 twinnings increase substantially by comparison with the pristine case and depend strongly on the twin orientation. The (101) twinning shows much larger thermal expansion than the (301) twinning. Further analysis indicates the physical mechanism can be mainly attributed to the effect of rotational degree of freedom of the SnO_6 octahedron motif and the stress induced by TGB. Our work reveals the physical mechanism underlying the distinct effect of TGB on thermal expansion caused by different chemical bonding, and meanwhile provides an insightful understanding of the relationship between specific structural features and thermal expansion in solid-phase materials.

DOI: 10.1103/PhysRevMaterials.6.083603

I. INTRODUCTION

Thermal expansion is the response of the volume of matter to temperature alterations. The vast majority of materials show positive thermal expansion with increasing temperature, as the asymmetric shape of the interatomic potential well (anharmonicity) leads to the increasing of bond distance, while few materials have anomalous negative thermal expansion that shrink in volume with increasing temperature, e.g., water near the freezing point [1–3]. Fine-tailoring thermal expansion of materials is crucial to the performance and accuracy of devices in engineering applications, especially aerospace and precision instruments [4,5]. The common strategy is to compose positive and negative thermal expansion materials to achieve near-zero or even zero thermal expansion [6–10]. The key is to discover the matching negative thermal expansion materials. The current research on the physical mechanism of negative thermal expansion mainly focuses on the intrinsic properties of materials [3,11,12]. Changes in the electronic structure of some materials with temperature, such as charge transfer (e.g., $SrCu_3Fe_4O_{12}$ [12] and $YbInCu_4$ [13]), ferroelectric phase transition (e.g., $PbTiO_3$ [14], $[PbTiO_3]_{0.4}$-$[BiFeO_3]_{0.6}$ [15]), magnetic reordering (e.g., Mn_3AN (A = Ni, Zn, Ga, Pd, and In) [16,17], $Zn_{0.85}Mn_{0.15}NMn_3$ [18]), cause the redistribution of charges, resulting in a large negative thermal expansion. In addition, some structure geometry changes of the open-framework structures with temperature (e.g., metal oxides, fluorides, and cyanides), such as the rotation of rigid structural units and the transverse vibration of bridging atoms, can also cause volume shrinkage [19–26]. In fluoride ScF_3, the rotation of the $[ScF_6]$ rigid units around covertices reduces the void in structure, causing a large negative expansion [27,28].

Defects are ubiquitous in materials and profoundly affect their physical properties. Recently, the twin grain boundary (TGB) gains more attention due to its significant influence on material properties (e.g., hardness, thermal transmission) [29–31]. As a typical surface defect, the TGB is widely present in polycrystalline solids. As illustrated in Fig. 1(a). the periodic arrangement of atoms is broken at the boundary and the interface between two crystalline grains orients in different directions. Electronic (e.g., charge distribution) and structural (e.g., the shape of rigid units) modifications are accommodated within the boundary area. It was observed that the 60° twin boundary in the layered chalcogenide material Bi_2Te_3 can act as a free electron creator, originating from the electronic structure modification at the boundary [32]. In addition, it found that twin boundaries in SnO_2 nanowires significantly reduce the coefficient of thermal expansion since twins compress the nearby hardened lattice [33]. The compress behavior results from a strong repulsion of the O-O bond at the twin boundary because the distance of the O-O bond at the boundary is shorter than that in the bulk. In addition, the rigid units are distorted at TGBs and potentially affect units' vibrational behavior [34,35]. Thus, the TGB provides a promising avenue to tune the thermal expansion properties

*fuyuhaoy@gmail.com
†lijun_zhang@jlu.edu.cn

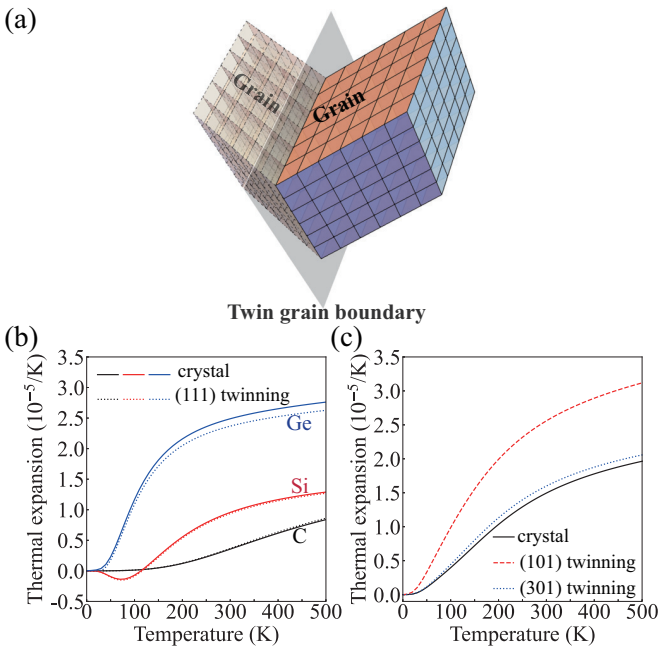

FIG. 1. (a) Illustration of the twin grain boundary. The CTE (α) dependent on temperature of (b) C/Si/Ge crystal/twinning, and (c) SnO_2 crystal, (101) twinning, and (301) twinning. The solid (dotted or dashed) line marks the crystal (twinning) thermal expansion.

of materials, even extending to other types of defects. To the best of our knowledge, there are few relevant studies, and the physical mechanism is not clear yet.

Here, we have studied the typical covalent bonding diamond (C; Si; Ge) twinning with the (111) TGB as well as the ionic bonding rutile (SnO_2, which usually acts as the electron transport layer of perovskite solar cells [36,37]) twinning with the (101) TGB and (301) TGB. Our goal is to illustrate the relationship between TGBs and thermal expansion. We find a slight relative change in thermal expansion for diamond structures introducing the (111) TGB compared to the corresponding crystal, primarily due to the modification of the vibrational phonon mode at the (111) TGB. The coefficient of thermal expansion (CTE) of both SnO_2 (101) twinning and (301) twinning is larger than that of crystal; especially (101) twinning, which is attributed to the reduction in the freedom degree of rotation of the SnO_6 octahedron and the distortion of octahedron at the TGB. As the rotational degree of freedom of the SnO_6 octahedron decreases, the thermal expansion increases. Meanwhile, for the SnO_2, twinning will decrease the bulk modulus of materials, which also has partially positive contribution to thermal expansion, e.g., 28%@(101) twinning. Moreover, because the atomic distance between oxygen atoms at the (101) TGB is shorter than that on both sides of the TGB in (101) twinning, the stress effect is induced.

II. COMPUTATIONAL METHODS

The density functional theory (DFT) calculations were performed with the projector augmented wave method [38] as implemented in the Vienna *ab initio* Simulation Package (VASP) [39–41]. The generalized gradient approximation of Perdew, Burke, and Ernzerhof [42] was adopted for the exchange-correlation functional. The kinetic energy cutoff of the plane-wave basis set was set to 520 eV, which ensures the energy converged to less than 1 meV/atom. The k-point meshes with grid spacing of $2\pi \times 0.03$ Å^{-1} were used for electronic Brillouin zone integration. We modeled the diamond (C, Si, and Ge) twinning with the (111) TGB and rutile (SnO_2) twinning with the (101) and (301) TGB by using our in-house developed codes [JAMIP (Jilin Artificial-intelligence aided Materials-design Integrated Package)] [43]. The structure optimizations were done with a tolerance on residual forces of 10^{-4} eV/Å. All of the relaxed twinning structures are well consistent with the previous reports [30,33–35,44,45].

The harmonic phonons were calculated by using the real-space supercell approach as implemented in the PHONOPY code [46]. The thermodynamics properties were calculated by the quasiharmonic approximation (QHA). In the QHA, the total Helmholtz free energy F can be approximately represented as [47]

$$F(V,T) = E_0(V) + F_{ph}(V,T) \tag{1}$$

and

$$F_{ph}(V,T) = -k_B T \ln \prod_{\mathbf{q},v} \frac{e^{-(1/2)\hbar\omega_{\mathbf{q},v}/k_B T}}{1 - e^{-\hbar\omega_{\mathbf{q},v}/k_B T}}, \tag{2}$$

where E_0 is the total static energy of the system at 0 K and F_{ph} is the Helmholtz free energy of lattice vibrations, depending on the phonon angular frequency $\omega_{\mathbf{q},v}$ and temperature T. k_B, $\hbar$, and V are the Boltzmann constant, reduced Planck constant, and volume, respectively. By fitting the energy versus volume curve based on the equation of state (e.g., Vinet [48], Birch [49], etc.), minimizing the Helmholtz free energy with respect to cell volume as a function of temperature can easily obtain the equilibrium volumes at different temperatures. Therefore, the volumetric thermal expansion coefficient α_V at T is written as [50]

$$\alpha_V(T) = \frac{V(T) - V_0}{V_0 T}, \tag{3}$$

where V_0 is the equilibrium volume at 0 K. Within the framework of QHA, the $\alpha_V(T)$ is also directly related to some thermodynamic properties through Grüneisen's relationship [1]

$$\alpha_V(T) = \frac{C_V(T)\bar{\gamma}(T)}{BV} \tag{4}$$

and

$$C_V(T) = \sum_{\mathbf{q},v} C_{\mathbf{q},v}, \tag{5}$$

$$C_{\mathbf{q},v} = k_B \left(\frac{\hbar\omega_{\mathbf{q},v}}{k_B T}\right)^2 \frac{e^{\hbar\omega_{\mathbf{q},v}/k_B T}}{[e^{\hbar\omega_{\mathbf{q},v}/k_B T} - 1]^2}, \tag{6}$$

$$\bar{\gamma}(T) = \frac{1}{C_V(T)} \sum_{\mathbf{q},v} \gamma_{\mathbf{q},v} C_{\mathbf{q},v}, \tag{7}$$

where C_V is the sum of the phonon mode heat capacity $C_{\mathbf{q},v}$, $\bar{\gamma}$ is the averaged Grüneisen parameter, B is the bulk modulus, V is the volume, and T is the temperature. The mode Grüneisen parameters are obtained by taking the logarithmic derivatives

of phonon frequencies with respect to volume change (i.e., through expanding/compressing the lattice with the strain $\delta\epsilon = \pm 1\%$. A phonon momenta q mesh of $20 \times 20 \times 20$ is used in the calculations of thermal properties to ensure that the thermal expansion α_V converges at the 1×10^{-7}/K level.

III. RESULTS AND DISCUSSION

We adopted the crystallographic structure information obtained by experiments to build the twinning structures [30,33–35,44,51]. The diamond (C, Si, and Ge) twinning structures with the (111) TGB were built as shown in Supplemental Material Fig. S1, of which the angle of TGB is around 142° [52]. The atoms near the interfaces maintained the 4-coordination as the bulk material, satisfying the eight-electron counting rule. Similarly, we adopted the (101) TGB @114° and (301) TGB@54.5° to model the rutile (SnO_2) twinning structures (Fig. S2) [52]. The coordination environment of Sn and O is also similar to that of its corresponding bulk phase. But, we noted that the connections of SnO_6 octahedra have some changes at the twin interfaces. We will discuss its effect on the thermal expansion properties later.

The temperature-dependent CTE of diamond (C, Si, and Ge) and rutile (SnO_2) were calculated as shown in Figs. 1(b) and 1(c), respectively. We found that compared with single crystal materials, twinning will cause the changes in the CTE of materials from increasing (e.g., C) to decreasing (e.g., Si and Ge) with the increase of atomic number. The introduction of twins in C and Si hardly changes the CTE of materials in the entire temperature range studied (< 500 K) while the CTE of Ge by twinning is significantly weakened above room temperature. In agreement with previous reports [53–55], we noted that both crystals and twins of silicon have weak negative thermal expansion at about 100 K. Conversely, the SnO_2 twinning both with (101) TGB and with (301) TGB we constructed show a tendency to increase thermal expansion, especially for the former. The presence of (101) TGB significantly increases the CTE of SnO_2 over almost the entire temperature range studied. It implies that the elimination of some specific twin boundary types, such as (101) TGB@SnO_2, may significantly improve the thermal failure issue of perovskite solar cells due to the large mismatch of thermal expansion properties between different functional layers.

The physical factors that may affect the CTE [see Eq. (4)] include heat capacity C_V, bulk modulus B, volume V, and the averaged Grüneisen parameters $\bar{\gamma}$, as shown in Sec. II of the Supplemental Material [52]. By comparing the available experimental thermal expansion data of the bulk materials, we found that our calculated thermal expansion coefficients show excellent agreement with the data of diamond C [Fig. S3(a)]. For Si, Ge, and SnO_2, our calculations exhibit slight overestimation (about 20%, 35%, and 21% at 300 K for Si, Ge, and SnO_2, respectively), compared with experimental data. Such slight underestimation caused by the QHA method would not affect our study of the effect of twin grain boundaries on the thermal expansion, taking into account systematic error cancellation between bulk and twin structures. We found that the twins and crystal have the same volumetric heat capacity C_V/V and bulk modulus B, except for the B@SnO_2 system (Fig. S5). Here, SnO_2 twins have a smaller B, implying

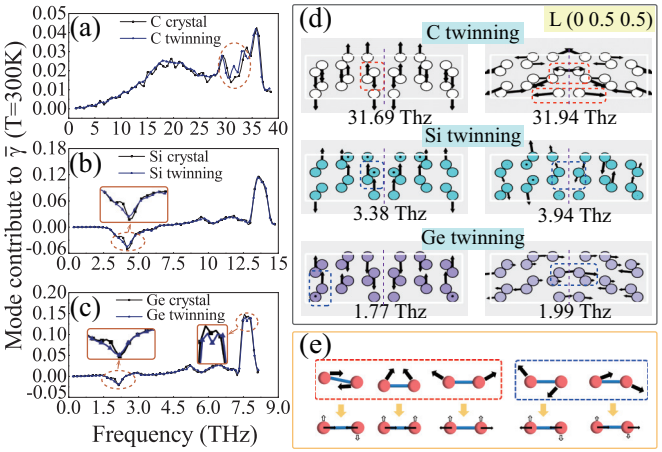

FIG. 2. (a)–(c) Cumulative Grüneisen parameters at different frequencies at 300 K. (d) The vibrational modes of some specific phonons at L (0, 0.5, 0.5) point around twin boundaries. (e) Schematic diagram of the vibrational modes. The tree modes in the red dashed box present the vibrational modes corresponding to positive thermal expansion; the two modes in the blue dashed box contribute to the negative thermal expansion.

their bulk moduli also have a positive contribution to thermal expansion. However, the reduction in bulk modulus only contributes about 28%@300 K according to the comparison of Fig. S5(d). It is not enough to explain that the thermal expansion of SnO_2 twins increases over 71%. Therefore it must be the $\bar{\gamma}$ that plays a central role in modulating thermal expansion properties in our studied systems.

It is well known that thermal expansion of materials is derived from the anhamonicity of lattice vibration. According to Eqs. (4)–(7), the more phonons having negative Grüneisen parameters (γ), the lower the CET of materials. When phonons with negative γ dominate ($\bar{\gamma} < 0$), the material exhibits negative thermal expansion. In other words, materials with negative averaged Grüneisen parameters ($\bar{\gamma}$) have negative thermal expansion. The phonon dispersions (0 K) and projected phonon densities of state of the diamond (C, Si, and Ge) crystal and twinning are given in Fig. S6 [52]. The mode-Grüneisen parameters are indicated on the dispersions. For C, no negative γ are observed in its crystals and twins. In contrast, for silicon and germanium, the introduction of twin boundaries leads to more phonons with negative γ in the low-frequency range (e.g., 5 THz@Si and 2.5 THz@Ge). Because of the strong bond energy of the C-C bond (346 kJ/mol), the bond at the TGB of C twinning remains unsoftened with increasing temperature. On the contrary, the weaker Si-Si bond (222 kJ/mol) and Ge-Ge bond (188 kJ/mol) are more sensitive to the twinning boundary and tend to soften as the temperature rises [56–58]. Interestingly, we found that for C, Si, and Ge, the calculated phonon densities of state of the crystals and twins are very similar [Figs. S6(c), (f), and (i)], suggesting that the twin boundary mainly affects the anharmonicity of material rather than the harmonic term.

We calculated the cumulative γ as a function of frequency at room temperature [Figs. 2(a)–2(c)]. The results show that the calculated cumulative $\gamma(\omega)$ of twins and crystals are similar in most frequency ranges, except for some

specific frequency regions. For C twins with (111) TGB, the slight increase in CTE with respect to crystals is mainly from the contribution of some high-frequency (∼31–35 THz) phonons, which have a larger γ (marked by the red dashed circle). Conversely, for Si and Ge twins, the low-frequency (∼3.3–4.2 THz@Si and ∼1.7–2.2 THz@Ge) phonons with more negative γ are the main reason for the decrease in thermal expansion. Unlike silicon, we noticed that Ge (111) twins have slightly increased positive cumulative $\gamma(\omega)$ in the high-frequency range (∼7.7–7.8 THz), partially offsetting the former's contribution to the reduction of thermal expansion. In additon, we projected the atomic vibration modes at the L (0, 0.5, 0.5) point, where the variation in γ between twins and crystals is more pronounced (Fig. S9) [52]. For C twinning, the atoms near the TGB vibrate oppositely along the bonding direction [marked by the red dashed box in the upper panel in Fig. 2(d)], and it can be regarded as normal phonon modes that contribute to positive thermal expansion. For Si/Ge twins, the atomic vibrations near the boundaries exhibit the shearlike modes [designated by the blue dashed box in the middle and lower panels in Fig. 2(d)], which is analogous to the tension effect in the negative thermal expansion materials [1,59,60]. Furthermore, we found that for these covalently bonded diamond (C, Si, and Ge) structures, the atomic vibrations can be divided into two categories with a total of five modes [Fig. 2(e)]. The first three modes contribute positive thermal expansion, including relatively large stretching vibration of bonds; the latter two contribute negative thermal expansion, having large bond shearing motion accompanied by small codirectional vibrations along the bonding direction. It should be emphasized that although the first mode contains a small shear component, the contribution of these modes to thermal expansion is very weak and can be ignored.

The C twins have a different lattice dynamics behavior than the Si and Ge twins. The main reason is that for diamond C, the introduction of twin boundaries does not significantly alter the chemical bonding around the boundaries due to the strong C-C bonds, which is consistent with the experimental finding that twinned diamond has a higher hardness than natural crystalline diamond [30]. In diamond C twins, the low-frequency phonons only exhibit vibrational behavior similar to those in bulk without shearing vibrational modes [53,54]. Conversely, high-frequency phonons with stretching vibration characteristics have high vibrational energy comparable to the bond energy of the C-C bond and become sensitive to the bonding environment since the strong C-C bond suppresses the transverse vibration of atoms. For Si and Ge twinning, the bond strength of the Si-Si and Ge-Ge bonds decreases rapidly compared to the C-C bond, as mentioned before [56–58]. These low-frequency shear phonons become sensitive to changes in covalent bonding. It results in these low-frequency phonons with more negative γ.

Figure 3(a) shows the calculated phonon dispersion of the SnO_2 crystal. We found that some low-frequency phonons have negative γ. For instance, we selected the first optical phonon at the S (−0.5, 0.5, 0) point with large negative γ, and its vibration mode corresponds to the rotation of corner-sharing SnO_6 octahedra (blue circles), resulting in the reduction of the interstitial space between the octahedrons [Fig. 3(b)]. The vibration characteristics of this mode are

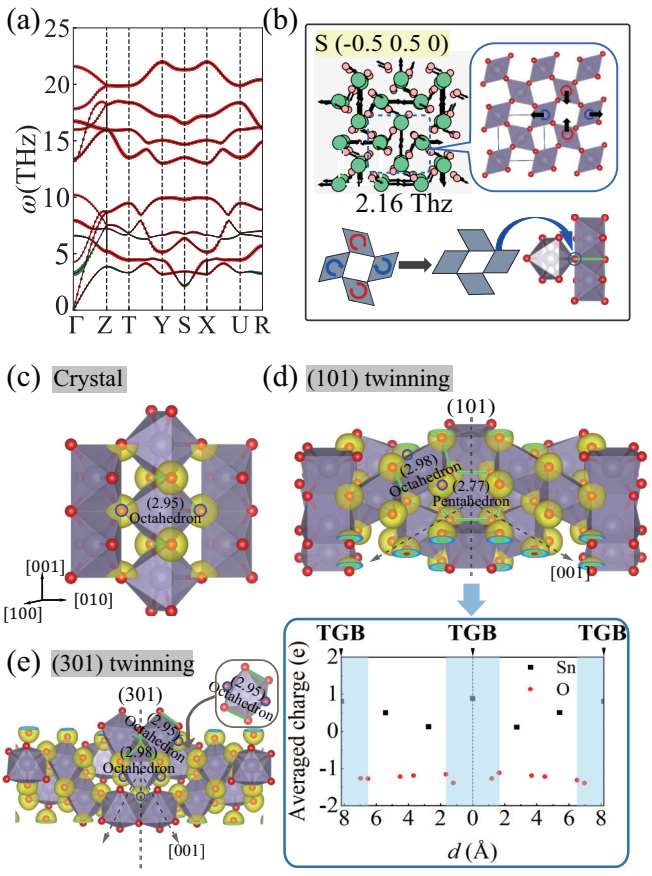

FIG. 3. (a) Calculated phonon dispersion of the SnO_2 crystal. (b) The low-frequency (2.16 THz) negative vibrational mode at S (−0.5, 0.5, 0) point. Two insets on the bottom and right illustrate the connection and vibration patterns of polyhedrons. The corresponding mean distance between oxygen atoms $\bar{d}_{O\text{-}O}$ in the polyhedrons of (c) the crystal, (d) (101) twinning, and (e) (301) twinning. The lower panel in (d): the charge distribution profile, i.e., the averaged Bader charge results along the direction perpendicular to the twining plane of the (101) TGB.

generally associated with negative thermal expansion in metal oxides and fluorides [19–23]. As portrayed in Fig. 3(c), the SnO_2 crystal is composed of SnO_6 octahedra that are connected by two covertices and two coedges (solid green lines). Due to the existence of the twin boundaries, the rotational freedom degree between octahedra is limited, and the bonding network of material is strengthened. Especially in the (101) twinning, no negative γ are observed [Fig. S7(b)] [52]. We found that the configurations of polyhedra at the boundary of SnO_2 twins are complex and strongly depend on the type of TGB. At the (101) TGB, the SnO_6 octahedron can be approximated as a pentahedron, forming four coedges (no covertex) with the adjacent octahedrons [Fig. 3(d)]. However, in (301) twins, there are two types of octahedrons [Fig. 3(e)]: one is at the TGB and consists of three covertices and two coedges; another is away from the TGB and contains one covertex and three coedges.

Several physical mechanisms have been proposed to explain the abnormal negative thermal expansion in materials, such as rigid unit modes [61,62], tension effect [1,59,60],

TABLE I. Averaged covertices and coedges per octahedron in SnO_2 crystal and twins. The numbers in brackets represent the number of atomic bilayers between the two parallel twin boundaries in the structure.

	Covertices	Coedges	CTE (ppm/K) at 300 K
Crystal	2	2	14.94
(301)[2]	1.83	2.35	15.99
(301)[1]	1.67	2.67	16.20
(101)[3]	1.50	2.50	23.49
(101)[2]	1.33	2.67	25.60

electronic phase transition [11,12], ferroelectric (magnetic ordering) phase transition [14–18,63,64], etc. To our best knowledge, descriptors that can efficiently predict the thermal expansion properties are still rarely reported [65,66]. Interestingly, we found that the number of covertices is a good descriptor for the rotational freedom degree of polyhedrons, which can be used to predict the thermal expansion properties in SnO_2 materials, while possibly extending to other similar systems. As shown in Fig. S10, the SnO_2 (101) and (301) twinnings have different lattice parameters, i.e., have different numbers of atomic bilayer between the twin boundaries. For a fair comparison, we counted all the covertices and coedges in the structure and then averaged the numbers of covertices and coedges per octahedron as listed in Table I. The results show an inverse relationship between the number of covertices and the CTE of material, i.e., the CTE increases with the decrease of the number of covertices.

The introduction of TGB in the material leads to the redistribution of charges, especially at the boundaries. Here, we choose the mean spacing of anions ($\bar{d}_{O\text{-}O}$) in the polyhedrons to evaluate the intensity of charge distribution as shown in Figs. 3(c)–3(e). For SnO_2 (101) twinning, the $\bar{d}_{O\text{-}O}$ at the TGB (2.77 Å) is shorter than those away from the boundaries (2.98 Å) and in the crystal (2.95 Å). However, for (301) twinning, the $\bar{d}_{O\text{-}O}$ at the TGB (2.98 Å) is comparable to its vicinity (2.95 Å) and in the crystal (2.95 Å). The Bader charge analysis [67–70] is performed to quantify the charge redistribution of the (101) twinning, as shown in the lower panel of Fig. 3(d). The results indicate that oxygen anions in the area of TGBs (shade areas) own more averaged charges than those away from boundaries. This is consistent with the substantially shortened $\bar{d}_{O\text{-}O}$ of (101) TGB, which indicates that oxygen anions at (101) TGB have strong stretching capacity. We noted that a similar phenomenon was recently reported experimentally in the SnO_2 twin nanowires by Zhu *et al.* [33].

The projected phonon densities of state of two twins and the crystal are given in Figs. 4(a)–4(c). In the SnO_2 crystal, the low-frequency peak of oxygen atoms [orange dashed box in Fig. 4(a)] are mainly from the phonons (~6.5 THz) at the R point, and they have negative γ values. The vibrational modes are mainly shear motion between neighboring O atoms [Fig. 4(d)], which cause the distortion of the octahedra and shrinkage of the volume. It is similar to the situation in the above Si/Ge twins. However, twinning leads to a blueshift in the vibrational frequencies of the oxygen atoms and hinders the shear motions in tin dioxides, resulting in the reduction [e.g., (301) twin] or even disappearance [e.g., (101) twin] of

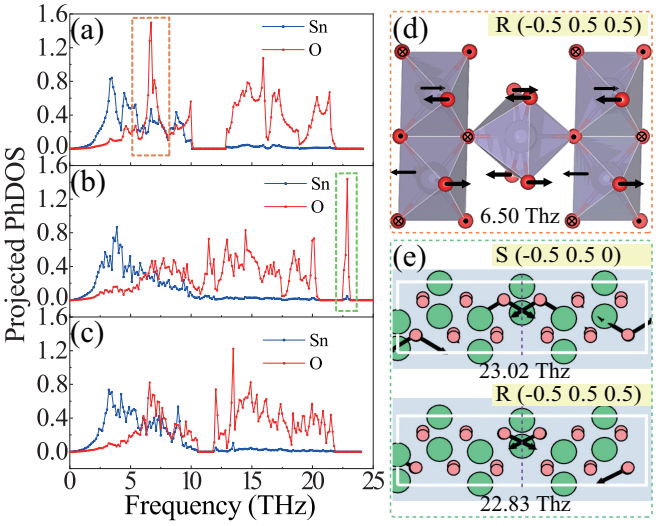

FIG. 4. Projected phonon densities of state of (a) crystal, (b) (101) twinning, and (c) (301) twinning. (d) The vibrational mode at the low-frequency peak (6.5 Thz) in the crystal. (e) The vibrational mode at the high-frequency peak (~23 Thz) in the (101) twinning.

phonons with negative γ. For instance, in (101) twinning, the vibration mode corresponding to the highest peak [green dashed box in Fig. 4(b)] contains a prominent stretching component [Fig. 4(e)], similar to the second mode in Fig. 2(e). It implies the presence of stress effect at the (101) TGB, encouraging positive thermal expansion with temperature.

Furthermore, we investigated the change of thermal expansion with the twin grain boundary density [71] based on a series of twin grain boundaries with different intervals, as shown in Fig. S12 [52]. We found that for the covalent solids (C, Si, and Ge), the thermal expansion coefficients show a small change with grain boundary density (within 5×10^{-6}/K per density unit 1/Å). For the ionic solid SnO_2, the (301) twinning shows slightly increased thermal expansion with decreasing grain boundary density ($< 2 \times 10^{-6}$/K per 1/Å), and the (101) twinning exhibits visibly increased thermal expansion with decreasing density (8×10^{-5}/K per 1/Å). The more sensitive variation of thermal expansion with grain boundary density in SnO_2 (101) twinning is ascribed to the wider effective region of the grain boundaries spreading [as indirectly reflected by the larger internal strain, i.e., the shorter mean spacing of O anions shown in Fig. 3(d)].

As known, the anharmonicity of materials changes the atomic vibrational potential well and affects thermal expansion as temperature rises [72–74]. The anharmonic effect can be reasonably described by the temperature-dependent effective potential method (TDEP) [75,76] that reconstructs second- and third-order interatomic force constants at finite temperatures by extracting the molecular dynamics simulation data. We attempted to adopt the TDEP method to evaluate the effect of anharmonicity on the thermal expansion of the twinning grain boundaries in this work. However, we found that while the TDEP method can reasonably describe bulk phase materials, it fails at dealing with the twinning grain boundaries, even for the simplest C/Si/Ge twinning (with 24 atoms unit cell). With the strenuous efforts we devoted

we still could not obtain the converged and stable phonon spectra without negative phonon frequencies for these twinnings, which implies that the TDEP method is not good at dealing with the systems having misbonded motifs or defects with quite low symmetry. The main underlying reason is that since the irreducible coefficients of the force constants are determined by solving a set of linear equations consisting of the atomic displacements and their induced forces, the number of irreducible coefficients to be solved depends on the symmetry of the structure. Meanwhile, because of the remarkably increased degrees of freedom for the atomic displacements in the low-symmetry twinning structures, the expensively time-consuming molecular dynamics with much more simulation steps is required to explore the more complex potential energy surface, as compared to the bulk phase case. Statistically averaging these complex potential energy surfaces to a simple potential (consisting of second- and third-order force constant terms) also poses a serious challenge, which results in an inaccurate and not reliable description of lattice dynamics and phonon properties.

We have adopted an alternative method [77] to qualitatively evaluate the anharmonic effect of the complex twinning structures involved in the current work through the average Grüneisen parameter $\bar{\gamma}$ at finite temperature T, as shown in Sec. VII of the Supplemental Material [52]. Since the thermal expansion is directly related to $\bar{\gamma}$ in terms of the Grüneisen relationship, we can evaluate to some extent the effect of anharmonicity on thermal expansion through investigating how the anharmonicity affects $\bar{\gamma}$. Two representative cases with covalent and ionic bondings [i.e., Si (111) and SnO_2 (101) twinning] were chosen for such calculations, as shown in Fig. S13. The results on corresponding bulk materials are shown for comparison. We found that for the covalent Si, the anharmonicity shows more influence on the twinning structure than on the bulk. Both the QHA and the anharmonicity cases demonstrate the same tendency in modulating $\bar{\gamma}$. The slightly decreasing thermal expansion from the bulk to twinning structure, which is captured by the QHA calculation [Fig. 1(b)], show consistency with the fact observed experimentally that the thermal expansion of polycrystalline silicon is slightly lower than that of monocrystal [78]. Turning to the ionic SnO_2, the results indicate that the anharmonicity demonstrates comparable weak effect on $\bar{\gamma}$ for the bulk to twinning structures at room temperature and above. This is in accordance with the experimental observation in SnO_2 single crystal that the anharmonic interactions among the phonons produce temperature-dependent phonon frequencies through mainly a pure-volume contribution which results from thermal expansion, whereas the pure-temperature contribution which results from cubic and quartic anharmonicities plays a minor role [79]. From the above analysis, we can reasonably speculate that the main conclusions reached by our QHA calculations will hold when the anharmonicity effect is fully included in future studies.

IV. CONCLUSION

To summarize, we investigated theoretically how the TGB affects thermal expansion in insulating solid materials by using first-principles calculations. For the covalent bonding materials represented by diamond-structure solids, we found the thermal expansion of the twinning structure shows a subtle change compared with that of pristine material, except that for Ge the twinning structure exhibits increasingly reduced thermal expansion with temperature. The atomic vibrational modes associated with the (111)-oriented TGB determine predominantly the change of the thermal expansion. In the case of C twinning, the high-frequency mode with opposite-direction atomic vibration in the C-C bond is enhanced, which slightly increases thermal expansion. For Si/Ge twinning, the low-frequency vibrational mode perpendicular to the bond direction becomes prevailing at the TGB. This mode restricts thermal expansion, analogous to the tension effect of the negative thermal expansion materials. In Ge the high-frequency mode with opposite-direction atomic vibration in the Ge-Ge bond shows reduced frequency, which further inhibits its thermal expansion. For the ionic bonding materials represented by rutile SnO_2, the thermal expansion of the twinning structure increases substantially by comparison with the pristine case and shows strong dependence on the twin orientation. The bulk modulus of twins is reduced compared to crystals, which contributes partly to their larger thermal expansion. The (101) twinning shows much larger thermal expansion than the (301) twinning. The different dependence of thermal expansion on the twin orientation is attributed to the reduced degree of freedom of SnO_6 octahedron rotation and the distortion of the SnO_6 octahedron in proximity to TGB. As the degree of freedom of SnO_6 octahedron rotation decreases, the thermal expansion shows an increasing behavior. For the (101) twinning, the stress effect causing distortion of the SnO_6 octahedron further facilitates the enhancement of thermal expansion.

It was reported by Zhu *et al*. that the SnO_2 nanowires containing the (101) TGB exhibit significantly reduced, even near-zero thermal expansion above room temperature by comparison with the bulk phase [33]. By analyzing the x-ray pair distribution function results, they claimed that with increasing temperature, (i) the longer Sn-O bonds in the nanowires with TGB remain almost constant, distinct from the bulk phase where the longer Sn-O bonds increase linearly; (ii) the O-Sn-O angles in the nanowires with TGB increase, compensating for the slight expansion caused by the shorter Sn-O bonds upon heating. In the Raman spectra study, it was observed that as the temperature rises the relevant phonon modes of nanowires show the feature of phonon stiffness, compared to the bulk ones. They performed the first-principles DFT calculation where the atoms within three layers of the Sn-O octahedra connection framework across the TGB are relaxed by local total energy minimization, and the other atoms are fixed. They found that for the optimized structure the O-O distance across the TGB reduces to 2.035 Å, much shorter than the 3.186 Å of the bulk phase. They proposed that the compressed oxygen sublattice causes the strong internal stress, which hardens the phonon modes, thus resulting in the weakening of thermal expansion. In our study, we simulated the TGB oriented along both the (101) and the (301) directions, which both exhibit enhanced thermal expansion compared with the bulk phase (Fig. 1). For the (101)-oriented TGB, our results indicate a remarkably enhanced thermal expansion that increases further with temperature. In our calculations, we fully relaxed all the atoms forming the TGB in the

periodic structure. For the (101)-oriented TGB case, the O-O distances across the TGB are 2.406 and 2.393 Å. Although the values are shorter than that of the bulk phase, they are much longer than the calculated value by Zhu *et al*. [33]. This indicates the existing moderate internal stress across the TGB. From Figs. 3(c)–3(e), it can be seen that the stress across the TGBs does cause substantial distortion of the local structure. However, in our calculations, these effects do not lead to the reduction of thermal expansion. The implication is that the phonon modes hardening, which is expected to be caused by the internal stress and its resulting distorted local structure, does not occur in our study. We speculate that a few factors may need to be considered to account for the discrepancy between our calculations and the experiments: The first one is the density of TGBs, which has a significant effect on the relaxation of the internal stress across the TGB, as well as the phonon modes and thermal expansion. Our calculations are carried out at the high-density condition because of the limitation of computational cost. We found a tendency of reduction of the thermal expansion by decreasing the TGB density (e.g., by slightly increasing the distance among TGBs in the periodic structure). The second one is the anharmonic effect, which may become conspicuous as the temperature rises [80–83]. However, as we analyzed before, the effect of the anharmonic effect on SnO_2 is mainly from pure-volume contribution [79], which can be captured by the QHA method. Finally, the twinning structure may have a complex texture in the actual materials [34,44], which exhibits complex stress distribution and local structure distortion. As the final remark, the specific structural features such as the average atomic volume [66] and the connection profile among polyhedron motifs discussed here, have shown a regulatory effect on the thermal expansion. The internal relationship between these specific structural features and thermal expansion deserves future studies from both experimental and theoretical efforts.

ACKNOWLEDGMENTS

This work was supported by the National Natural Science Foundation of China (Grants No. 12004131, No. 22090044, and No. 11674121), and Graduate Innovation Fund of Jilin University (Grant No. 101832020CX145). Calculations were performed in part at the high-performance computing center of Jilin University.

[1] G. D. Barrera, J. A. O. Bruno, T. H. K. Barron, and N. L. Allan, J. Phys.: Condens. Matter **17**, R217 (2005).
[2] J. S. O. Evans, J. Chem. Soc. Dalton Trans. **0**, 3317 (1999).
[3] K. Takenaka, Front. Chem. **6**, 267 (2018).
[4] X. Yuan, Y. Sun, H. Guo, K. Shi, P. Song, H. Han, J. Cui, S. An, R. Huang, L. Li, and C. Wang, Mater. Des. **203**, 109591 (2021).
[5] M. Lalpoor, D. G. Eskin, and L. Katgerman, Int. J. Mater. Res. **102**, 1286 (2011).
[6] L. Ding, C. Wang, Y. Na, L. Chu, and J. Yan, Scr. Mater. **65**, 687 (2011).
[7] K. Takenaka, T. Hamada, D. Kasugai, and N. Sugimoto, J. Appl. Phys. **112**, 083517 (2012).
[8] K. Takenaka and M. Ichigo, Compos. Sci. Technol. **104**, 47 (2014).
[9] X. Yan, J. Miao, J. Liu, X. Wu, H. Zou, D. Sha, J. Ren, Y. Dai, J. Wang, and X. Cheng, J. Alloys Compd. **677**, 52 (2016).
[10] D. Cen, B. Wang, R. Chu, Y. Gong, G. Xu, F. Chen, and F. Xu, Scr. Mater. **186**, 331 (2020).
[11] J. R. Salvador, F. Guo, T. Hogan, and M. G. Kanatzidis, Nature (London) **425**, 702 (2003).
[12] I. Yamada, K. Tsuchida, K. Ohgushi, N. Hayashi, J. Kim, N. Tsuji, R. Takahashi, M. Matsushita, N. Nishiyama, T. Inoue, T. Irifune, K. Kato, M. Takata, and M. Takano, Angew. Chem., Int. Ed. **50**, 6579 (2011).
[13] B. Kindler, D. Finsterbusch, R. Graf, F. Ritter, W. Assmus, and B. Lüthi, Phys. Rev. B **50**, 704 (1994).
[14] G. Shirane and S. Hoshino, J. Phys. Soc. Jpn. **6**, 265 (1951).
[15] J. Chen, X. R. Xing, G. R. Liu, J. H. Li, and Y. T. Liu, Appl. Phys. Lett. **89**, 101914 (2006).
[16] T. Hamada and K. Takenaka, J. Appl. Phys. **109**, 07E309 (2011).
[17] K. Takenaka and H. Takagi, Appl. Phys. Lett. **87**, 261902 (2005).
[18] J. C. Lin, P. Tong, W. Tong, Y. M. Zou, C. Yang, F. Zhu, X. K. Zhang, L. F. Li, M. Wang, Y. Wu, S. Lin, W. H. Song, X. B. Zhu, and Y. P. Sun, Scr. Mater. **152**, 6 (2018).
[19] V. Gava, A. L. Martinotto, and C. A. Perottoni, Phys. Rev. Lett. **109**, 195503 (2012).
[20] T. A. Mary, J. S. O. Evans, T. Vogt, and A. W. Sleight, Science **272**, 90 (1996).
[21] T. Chatterji, P. F. Henry, R. Mittal, and S. L. Chaplot, Phys. Rev. B **78**, 134105 (2008).
[22] Y. Oba, T. Tadano, R. Akashi, and S. Tsuneyuki, Phys. Rev. Materials **3**, 033601 (2019).
[23] D. Wendt, E. Bozin, J. Neuefeind, K. Page, W. Ku, L. Wang, B. Fultz, A. V. Tkachenko, and I. A. Zaliznyak, Sci. Adv. **5**, eaay2748 (2019).
[24] K. W. Chapman, P. J. Chupas, and C. J. Kepert, J. Am. Chem. Soc. **128**, 7009 (2006).
[25] A. L. Goodwin and C. J. Kepert, Phys. Rev. B **71**, 140301(R) (2005).
[26] N. C. Burtch, S. J. Baxter, J. Heinen, A. Bird, A. Schneemann, D. Dubbeldam, and A. P. Wilkinson, Adv. Funct. Mater. **29**, 1904669 (2019).
[27] B. K. Greve, K. L. Martin, P. L. Lee, P. J. Chupas, K. W. Chapman, and A. P. Wilkinson, J. Am. Chem. Soc. **132**, 15496 (2010).
[28] Y. Liu, Z. Wang, M. Wu, Q. Sun, M. Chao, and Y. Jia, Comput. Mater. Sci. **107**, 157 (2015).
[29] P. Uttam, V. Kumar, K.-H. Kim, and A. Deep, Mater. Des. **192**, 108752 (2020).
[30] Q. Huang, D. Yu, B. Xu, W. Hu, Y. Ma, Y. Wang, Z. Zhao, B. Wen, J. He, Z. Liu, and Y. Tian, Nature (London) **510**, 250 (2014).
[31] Y. Zhou, J.-Y. Yang, L. Cheng, and M. Hu, Phys. Rev. B **97**, 085304 (2018).

[32] K.-C. Kim, J. Lee, B. K. Kim, W. Y. Choi, H. J. Chang, S. O. Won, B. Kwon, S. K. Kim, D.-B. Hyun, H. J. Kim, H. C. Koo, J.-H. Choi, D.-I. Kim, J.-S. Kim, and S.-H. Baek, Nat. Commun. **7**, 12449 (2016).

[33] H. Zhu, Q. Li, C. Yang, Q. Zhang, Y. Ren, Q. Gao, N. Wang, K. Lin, J. Deng, J. Chen, L. Gu, J. Hong, and X. Xing, J. Am. Chem. Soc. **140**, 7403 (2018).

[34] V. Hrkac, N. Wolff, V. Duppel, I. Paulowicz, R. Adelung, Y. K. Mishra, and L. Kienle, Appl. Microsc. **49**, 1 (2019).

[35] W.-Y. Lee, P. D. Bristowe, Y. Gao, and K. L. Merkle, Philos. Mag. Lett. **68**, 309 (1993).

[36] Q. Jiang, X. Zhang, and J. You, Small **14**, 1801154 (2018).

[37] J. Kim, K. S. Kim, and C. W. Myung, npj Comput. Mater. **6**, 100 (2020).

[38] P. E. Blöchl, Phys. Rev. B **50**, 17953 (1994).

[39] G. Kresse, J. Non-Cryst. Solids **192-193**, 222 (1995).

[40] G. Kresse and J. Furthmüller, Comput. Mater. Sci. **6**, 15 (1996).

[41] G. Kresse and D. Joubert, Phys. Rev. B **59**, 1758 (1999).

[42] J. P. Perdew, K. Burke, and M. Ernzerhof, Phys. Rev. Lett. **77**, 3865 (1996).

[43] X.-G. Zhao, K. Zhou, B. Xing, R. Zhao, S. Luo, T. Li, Y. Sun, G. Na, J. Xie, X. Yang, X. Wang, X. Wang, X. He, J. Lv, Y. Fu, and L. Zhang, Sci. Bull. **66**, 1973 (2021).

[44] H. Iwanaga, M. Egashira, K. Suzuki, M. Ichihara, and S. Takeuchi, J. Mater. Sci. Lett. **8**, 1179 (1989).

[45] X. Liu, L. Liu, X. Wu, and P. K. Chu, Phys. Lett. A **379**, 1384 (2015).

[46] A. Togo and I. Tanaka, Scr. Mater. **108**, 1 (2015).

[47] A. Togo, L. Chaput, I. Tanaka, and G. Hug, Phys. Rev. B **81**, 174301 (2010).

[48] P. Vinet, J. H. Rose, J. Ferrante, and J. R. Smith, J. Phys.: Condens. Matter **1**, 1941 (1989).

[49] F. Birch, Phys. Rev. **71**, 809 (1947).

[50] W. Miller, C. W. Smith, D. S. Mackenzie, and K. E. Evans, J. Mater. Sci. **44**, 5441 (2009).

[51] J. Narayan and A. S. Nandedkar, Philos. Mag. B **63**, 1181 (1991).

[52] See Supplemental Material at http://link.aps.org/supplemental/10.1103/PhysRevMaterials.6.083603 for details on twinning structures, comparison between calculated and experimental values of physical factors (including bulk modulus, heat capacity, Grüneisen parameter, and thermal expansion coefficients), phonon dispersion, variation of thermal expansion coefficients with the density of twin boundary, and analysis of anharmonic effect.

[53] C. H. Xu, C. Z. Wang, C. T. Chan, and K. M. Ho, Phys. Rev. B **43**, 5024 (1991).

[54] S. Biernacki and M. Scheffler, Phys. Rev. Lett. **63**, 290 (1989).

[55] K. Yang, J. Xiao, J.-W. Luo, S.-S. Li, S.-H. Wei, and H.-X. Deng, New J. Phys. **21**, 123015 (2019).

[56] T. Cottrell, *The Strengths of Chemical Bonds* (Butterworths, London, 1954).

[57] S. W. Benson, J. Chem. Educ. **42**, 502 (1965).

[58] B. d. Darwent, *Bond Dissociation Energies in Simple Molecules* (National Standard Reference Data System, 1970).

[59] A. Sanson, Solid State Sci. **11**, 1489 (2009).

[60] L. H. N. Rimmer, M. T. Dove, B. Winkler, D. J. Wilson, K. Refson, and A. L. Goodwin, Phys. Rev. B **89**, 214115 (2014).

[61] K. Takenaka, Sci. Tech. Adv. Mater. **13**, 013001 (2012).

[62] J. N. Grima, M. Bajada, S. Scerri, D. Attard, K. K. Dudek, and R. Gatt, Proc. Math. Phys. Eng. Sci. **471**, 20150188 (2015).

[63] K. Takenaka, M. Ichigo, T. Hamada, A. Ozawa, T. Shibayama, T. Inagaki, and K. Asano, Sci. Tech. Adv. Mater. **15**, 015009 (2014).

[64] C. Wang, L. Chu, Q. Yao, Y. Sun, M. Wu, L. Ding, J. Yan, Y. Na, W. Tang, G. Li, Q. Huang, and J. W. Lynn, Phys. Rev. B **85**, 220103(R) (2012).

[65] J. T. Schick, A. M. Gopakumar, and A. M. Rappe, arXiv:1701.03966.

[66] Q. Gao, J. Wang, A. Sanson, Q. Sun, E. Liang, X. Xing, and J. Chen, J. Am. Chem. Soc. **142**, 6935 (2020).

[67] G. Henkelman, A. Arnaldsson, and H. Jónsson, Comput. Mater. Sci. **36**, 354 (2006).

[68] E. Sanville, S. D. Kenny, R. Smith, and G. Henkelman, J. Comput. Chem. **28**, 899 (2007).

[69] W. Tang, E. Sanville, and G. Henkelman, J. Phys.: Condens. Matter **21**, 084204 (2009).

[70] M. Yu and D. R. Trinkle, J. Chem. Phys. **134**, 064111 (2011).

[71] N. Bozzolo and M. Bernacki, Metall. Mater. Trans. A **51**, 2665 (2020).

[72] D. C. Wallace, Phys. Rev. **139**, A877 (1965).

[73] T. R. Ravindran, A. K. Arora, and T. A. Mary, Phys. Rev. B **67**, 064301 (2003).

[74] E. Liang, Q. Sun, H. Yuan, J. Wang, G. Zeng, and Q. Gao, Front. Phys. **16**, 53302 (2021).

[75] D. S. Kim, O. Hellman, J. Herriman, H. L. Smith, J. Y. Y. Lin, N. Shulumba, J. L. Niedziela, C. W. Li, D. L. Abernathy, and B. Fultz, Proc. Natl. Acad. Sci. USA **115**, 201707745 (2018).

[76] O. Hellman, I. A. Abrikosov, and S. I. Simak, Phys. Rev. B **84**, 180301(R) (2011).

[77] W. Li, J. Carrete, N. A. Katcho, and N. Mingo, Comput. Phys. Commun. **185**, 1747 (2014).

[78] H. Kahn, R. Ballarini, and A. H. Heuer, J. Mater. Res. **17**, 1855 (2002).

[79] P. S. Peercy and B. Morosin, Phys. Rev. B **7**, 2779 (1973).

[80] M. K. Gupta, R. Mittal, S. L. Chaplot, and S. Rols, J. Appl. Phys. **115**, 093507 (2014).

[81] G. Leibfried and W. Ludwig, Solid State Phys. **12**, 275 (1961).

[82] D. Bansal, J. Hong, C. W. Li, A. F. May, W. Porter, M. Y. Hu, D. L. Abernathy, and O. Delaire, Phys. Rev. B **94**, 054307 (2016).

[83] Y. Shen, C. N. Saunders, C. M. Bernal, D. L. Abernathy, M. E. Manley, and B. Fultz, Phys. Rev. Lett. **125**, 085504 (2020).